NJC

PAPER

View Article Online
View Journal | View Issue

Cite this: *New J. Chem.*, 2024, **48**, 11035

Unlocking the potential of $NiCo_2O_4$ nanocomposites: morphology modification based on urea concentration and hydrothermal and calcination temperature

Ataollah Niyati,* Arianna Moranda, Juan Felipe Basbus and Ombretta Paladino

Received 5th April 2024,
Accepted 21st May 2024

DOI: 10.1039/d4nj01581a

rsc.li/njc

Oxygen evolution reaction (OER) electrocatalysts are critical in minimizing energy loss during the anodic four-electron transfer process that is required for water oxidation. Improving and selecting optimal non-noble OER electrocatalysts are key strategies for elevating their overall performance and efficiency of energy storage and conversion. Eight $NiCo_2O_4$ electrocatalysts were synthesized using the hydrothermal method by changing the amount of urea as a nucleation agent and hydrothermal and calcination temperature to achieve an outstanding catalyst in terms of morphology and electrochemical activity. For examining the physicochemical properties of the electrocatalyst, analyses such as XRD, SEM, TEM, and EDS were conducted. Although XRD analysis revealed the formation of pure $NiCo_2O_4$ for all eight samples, SEM and TEM analysis unraveled the best electrocatalyst in terms of morphology to be NiCo-S3 (urea: 10 times higher, $T_{\text{hydrothermal}}$: 120 °C, and $T_{\text{Calcination}}$: 350 °C) and NiCo-S4 (urea: 10 times higher, $T_{\text{hydrothermal}}$: 120 °C, and $T_{\text{Calcination}}$: 400 °C) with a mum-flower-like shape and particle dimension between 20 and 45 nm. NiCo-S4 displayed robust electrochemical activity, primarily in the OER, with an overpotential of 327 mV at 10 mA cm^{-2} in 1.0 M aqueous KOH solution. The OER performance was enhanced as demonstrated by the exceptional durability of >24 hours and a Tafel slope of 79.7 mV dec^{-1}. Electrochemical impedance spectroscopy (EIS) revealed a low resistance of 1.03 Ω and a double-layer capacitance of 2.43 mF cm^{-2}, substantiating the outstanding OER performance of NiCo-S4.

1. Introduction

In recent years, the issue of energy storage has become increasingly important, and to simultaneously protect the environment and promote economic growth, some efforts should be made.[1] The growing concerns about global warming and the depletion of fossil fuels have made it clear that we need to prioritize the development of methods by leveraging renewable energy sources.[2–4] As a result, there is a growing demand for technologies that can efficiently collect, store, and use energy.[5] In view of this, electrochemical conversion and energy storage technologies such as water electrolysis, fuel cells, and redox flow batteries can address the problems by employing renewable energy sources such as solar, wind, and wave energy, thus enabling the storage and utilization of energy for power supply.[6–9] Hydrogen, a carbon-neutral form of energy, can be electrocatalytically produced *via* water electrolysis, stored and used as a fuel source in power generation devices whenever needed.[10] With reference to these technologies, the OER on the anode side is a crucial step in producing hydrogen.[11] For instance, concerning water electrolysis, identifying a good OER electrocatalyst is of the utmost importance because it plays a fundamental role in minimizing energy loss at the anode due to the four-electron transfer during water oxidation.[12] By selecting, studying, and improving OER electrocatalysts, we can significantly enhance the overall performance and efficiency of energy storage and conversion systems.[13]

Many studies have been conducted on transition metal oxides operating as oxygen evolution anodes under alkaline conditions, and they demonstrated appropriate overpotential and stability.[14–16] Spinel electrocatalysts, a type of transition metal oxide represented by the AB_2O_4 formula (A and B are metal ions), have garnered considerable interest for their potential applications as OER electrodes in water electrolyzers owing to their unique chemical makeup, structure, valence, and morphology.[17–19] $NiCo_2O_4$, more commonly referred to as cobalt–nickel oxide, is an extraordinary spinel catalyst due to its high capacity, excellent redox activity, affordability, and abundant availability in nature, which makes it highly desirable for use in the energy storage sector.[20,21] To be more precise, $NiCo_2O_4$ is composed of mixed-valence transition metal oxides

Department of Civil, Chemical and Environmental Engineering, University of Genoa (UNIGE-DICCA), Via All'Opera Pia 15, 16145 Genoa, Italy.
E-mail: ataollah.niyati@edu.unige.it

in which nickel occupies the octahedral sites, whereas cobalt occupies both the octahedral and tetrahedral sites.[22] Although $NiCo_2O_4$ has strong characteristics, the particle size and morphology are vital, especially in systems with porous conductive substrates as an anode and electrocatalysts as a reactive layer. As a result, the appropriate shape and size of the electrocatalyst should be in a way that does not block the pore sites of the substrate, allowing water and generated oxygen to pass easily without adding additional resistance to the system and, more crucially, improving electrocatalytic activity.[23]

A variety of techniques to synthesize $NiCo_2O_4$ spinel have been developed, including hydroxide decomposition,[24] nano casting,[25] electrodeposition,[26] coprecipitation,[27] and hydrothermal synthesis.[28] Among these methods, hydrothermal synthesis seems suitable for controlling the shape and producing a catalyst that can be used for deposition onto the surface of different substrates.[29–33] The hydrothermal method using a hydrolysis agent such as urea can make the desired morphology of the final electrocatalyst by the production of hydroxide in the solution which can firstly decompose the precursor salts and in the second step bond with Ni^{2+} and Co^{2+}, producing double-layered hydroxide (LDH) of Ni and Co, which can with thermal treatment produce pure single phase $NiCo_2O_4$.[34,35]

$NiCo_2O_4$ has been synthesized in a wide variety of structural forms, spanning nanoparticles,[36] nanowires,[37] nanoflowers,[38] nanosheet arrays,[39] and nanoneedle arrays,[40] and the results of these studies demonstrate the important role of shape in electrochemical characteristics.[41] The essential truth is that most of the manufactured $NiCo_2O_4$ electrocatalysts do not have a single morphology, consisting of a combination of rods and sheets, which may be ineffective when sprayed on conductive substrates for OER applications.

To overcome this issue, a hydrothermal method followed by a tempering step was used to construct $NiCo_2O_4$ with a finely controlled morphology for its use as an electrocatalyst in the OER. Three important factors were investigated in this work to optimize the material's morphology, *i.e.* hydrothermal temperature, calcination temperature, and the quantity of urea, which is used as a nucleation agent, facilitating the controlled release of metal ions and contributing to the formation of catalytically active sites. Furthermore, the electrochemical performance of the salient samples was thoroughly studied in order to determine the most promising contender. Several characterization techniques were used to provide a thorough understanding of the morphology and purity of the synthesized materials.

2. Experimental

2.1. Materials

$NiCl_2 \cdot 6H_2O$ (99% purity) as a Ni precursor, $CoCl_2 \cdot 6H_2O$ (98% purity) as a Co precursor, KOH (99% purity), and urea (99% purity) were acquired from Carlo Erba in order to make the requisite electrocatalysts. Ultra-pure deionized water was used for all cleaning and synthesis methods, which was purchased from Exaxol (Genova, Italy). Ethanol and acetone, which were used after filtration of electrocatalysts to remove any remaining residue, were purchased from Sigma Aldrich. To be more precise, all the reactants were used without further purification.

2.2. Preparation of $NiCo_2O_4$ nano electrocatalysts

The attainment of an electrocatalyst with a suitable morphology that can be readily deposited onto diverse electrodes without obstructing the desired electrode's pore structure is crucial. In order to address this requirement, three factors, namely, urea amount as factor 1, hydrothermal temperature as factor 2, and calcination temperature as factor 3, were systematically varied and investigated during the synthesis of $NiCo_2O_4$. A total of eight samples were synthesized and designated as NiCo-S1 to NiCo-S8, each exhibiting distinct characteristics, as outlined in Table 1. These modifications enable a comprehensive study of the influence of these factors on the morphology and properties of the $NiCo_2O_4$ electrocatalyst. Fig. 1 illustrates the synthesis procedure employed for the fabrication of $NiCo_2O_4$ using a facile hydrothermal method at a temperature of 120 °C or 180 °C, followed by subsequent calcination at 350 °C or 400 °C. The total amount of final powder obtained for each catalyst was 2 grams of $NiCo_2O_4$. The synthesis procedure involved several steps. Initially, 2.015 grams of $NiCl_2 \cdot 6H_2O$ was dissolved in 25 mL of deionized water (DI) and gradually added drop by drop to the $CoCl_2 \cdot 6H_2O$ solution, which contained 4.0354 grams of Co precursor and 40 mL of DI. In the second step, urea was added in two different quantities, namely, in a 1 : 2 and a 1 : 10 molar ratio, and the solution was vigorously stirred for 30 minutes. Subsequently, the solution was subjected to sonication in a bath for an additional 30 minutes to promote better nucleation and the formation of nanoparticles. The resulting solution was then transferred to a 100 mL Teflon-lined stainless-steel autoclave for the hydrothermal reaction, which was carried out for a duration of 10 hours. After the completion of the reaction, the powder was collected after washing with DI and ethanol. The collected powder was then filtered and dried in a vacuum oven at 60 °C. In the final step, the dried powder was placed in a furnace and subjected to a thermal treatment at either 350 °C or 400 °CC for a period of 3 hours, with a heating ramp of 10 °C min^{-1}. This process ensured the successful synthesis of $NiCo_2O_4$ with the desired characteristics for subsequent analysis and application.

2.3. Characterization of $NiCo_2O_4$ nano electrocatalysts

Several analytical techniques were used to analyze the materials' physical and chemical structure. X-ray diffraction (XRD)

Table 1 Names and different synthesis conditions

Name	Catalyst	Urea	$T_{Hydrothermal}$	$T_{Calcination}$
NiCo-S1	$NiCo_2O_4$	1 : 2	120	350
NiCo-S2	$NiCo_2O_4$	"	"	400
NiCo-S3	$NiCo_2O_4$	1 : 10	"	350
NiCo-S4	$NiCo_2O_4$	"	"	400
NiCo-S5	$NiCo_2O_4$	1 : 2	180	350
NiCo-S6	$NiCo_2O_4$	"	"	400
NiCo-S7	$NiCo_2O_4$	1 : 10	"	350
NiCo-S8	$NiCo_2O_4$	"	"	400

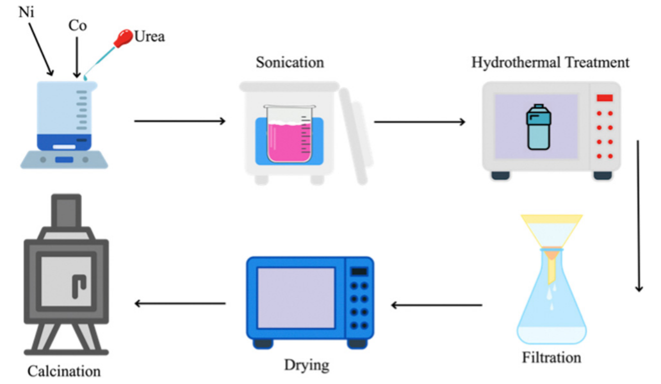

Fig. 1 Fabrication of $NiCo_2O_4$ nano electrocatalysts.

studies were carried out at room temperature in air using a PANalytical AERIS equipment to investigate the crystal structure and content. With the aid of scanning electron microscopy (SEM), the morphology of the samples was evaluated by using a TESCAN device. Using energy-dispersive spectroscopy (EDS) with a Hitachi SU3500 detector, it was possible to analyze the composition of $NiCo_2O_4$ and possible impurities in the synthesized samples. To examine the intricate structure and morphology, transmission electron microscopy (TEM) was carried out utilizing a JEM 2100 Plus by JEOL Ltd (Japan).

2.4. Electrochemical characterization

Electrocatalyst measurements were conducted using an IVIUM Vertex.10A potentiostat workstation (Ivium Technologies B.V., Netherlands) in a 1 M KOH electrolyte solution. The working electrode consisted of the $NiCo_2O_4$ deposited onto the Ni-felt by just putting a bare Ni felt inside the reaction reactor, while a Hg/HgO electrode served as the reference electrode, and a platinum wire was utilized as the counter electrode. The polarization curves were recorded at a scan rate of 5 mV s^{-1}. To determine the double-layer capacitance (C_{dl}), cyclic voltammograms (CVs) were obtained by varying the scan rates within a limited potential range. Electrochemical impedance spectroscopy (EIS) was performed over a frequency range spanning from 0.01 to 100 000 Hz. The time-dependent potential response was measured over a period of 24 hours, specifically under a current of 10 mA. All the reported potentials were calibrated with respect to a reversible hydrogen electrode (RHE) and were adjusted for the 80% iR drop using the equation $E(\text{RHE}) = E(\text{Hg/HgO}) + 0.927\ \text{V} - iR_s$, where R_s represents the equivalent series resistance derived from fitting calculations.[42]

3. Results and discussion

3.1. Mum flower-like $NiCo_2O_4$ nano electrocatalyst characterization

3.1.1. XRD analysis. In the context of materials characterization, XRD analysis is an essential tool utilized to acquire insights into the crystal structure and composition of synthetic materials. The XRD pattern of the synthesized powder has been recorded at 2θ = 20–80° for all samples, and samples NiCo-S2, NiCo-S3, NiCo-S4, NiCo-S6, and NiCo-S8 are shown in Fig. 2. For all samples, the peaks observed at 18.90°, 31.15°, 36.70°, 38.40°, 44.62°, 55.43°, 59.09°, 64.98°, and 77.54° were assigned to the (111), (220), (311), (222), (400), (422), (511), (440), and (533) crystallographic planes of cubic $NiCo_2O_4$, respectively, and the table is presented below. The obtained XRD pattern exhibited a strong agreement with the JCPDS 20-0781 standard card, providing concrete evidence for the successful formation of pure $NiCo_2O_4$ powders through the hydrothermal synthesis method. Importantly, no distinctive impurity peaks were detected, indicating the attainment of pure $NiCo_2O_4$ without significant contamination from other phases. Considering 2θ = 36.70° as the principal peak of the samples, the intensity of the peaks is decreased and broadened by increasing the factor 2 (Fig. 2, by comparing NiCo-S4 and NiCo-S8 and also comparing NiCo-S2 with NiCo-S6), as well as increasing the factor 1 (Fig. 2, by comparing NiCo-S2 and S4), which correlates with the smaller crystal size. In this case, the particle size of NiCo-S8 is more likely to be smaller than that of NiCo-S2, yet the particles can easily agglomerate and form a large grain, which can be observed *via* SEM examination. On the contrary, regarding factor 3, it is not possible with XRD analysis to conclude whether it can have an effect on morphology and particle size or not, so further analysis such as TEM analysis and electrochemical activity tests have been taken into account.

3.1.2. Morphology analyses. The utilization of SEM analysis emphasizes the structure, particle size, and distribution of produced nanomaterials. SEM characterization has been performed on all samples, and in Fig. 3, SEM analysis for NiCo-S2, NiCo-S3, NiCo-S4, NiCo-S6, and NiCo-S8 is shown. According to

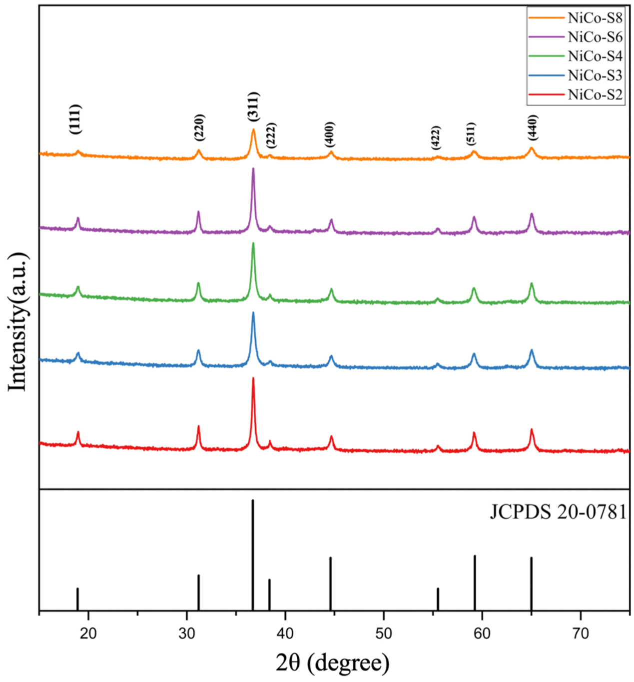

Fig. 2 XRD patterns of 8 samples of $NiCo_2O_4$ synthesized under different conditions.

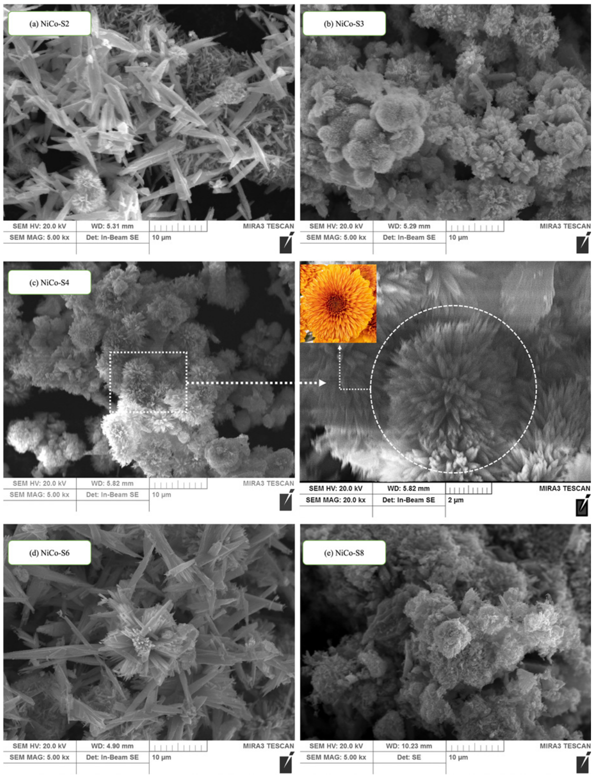

Fig. 3 SEM images of $NiCo_2O_4$ synthesised under different conditions: (a) NiCo-S2, (b) NiCo-S3, (c) NiCo-S4, (d) NiCo-S6 and (e) NiCo-S8.

the results of the SEM investigation, the comparison of images in Fig. 3(b) and (c) with those in Fig. 3(a), (d), and (e) points out that they have an identical single-phase morphology with a unique urchin-like shape. To be more specific, they form a mum-flower structure, which is composed of multiple rods. The quantity of urea as factor 1 used during the production has an important effect on the form of these flower-like structures. An increase in factor 1 promotes nucleation by acting as a hydrolysis agent for Ni^{2+} and Co^{2+} ions, allowing them to bind and form a unified shape. Furthermore, increasing factor 2 causes the production of various morphologies in addition to rod-like structures. These alternate geometries, however, are less appropriate for the catalysts used on different substrates and their spraying because they can block the pore sites. Additional characterization techniques, such as TEM and electrochemical characterization, are reported to offer an in-depth examination of factor 3.

The results of an EDS examination are shown in Fig. 4 for two samples: (a) NiCo-S3 and (b) NiCo-S4. Ni, Co, and O elements have been identified using EDS in three different zones. It is evident that the percentage of Ni, Co, and O is nearer the $NiCo_2O_4$ theoretical composition, which confirms the accurate synthesis and dispersion of elements in these electrocatalysts.

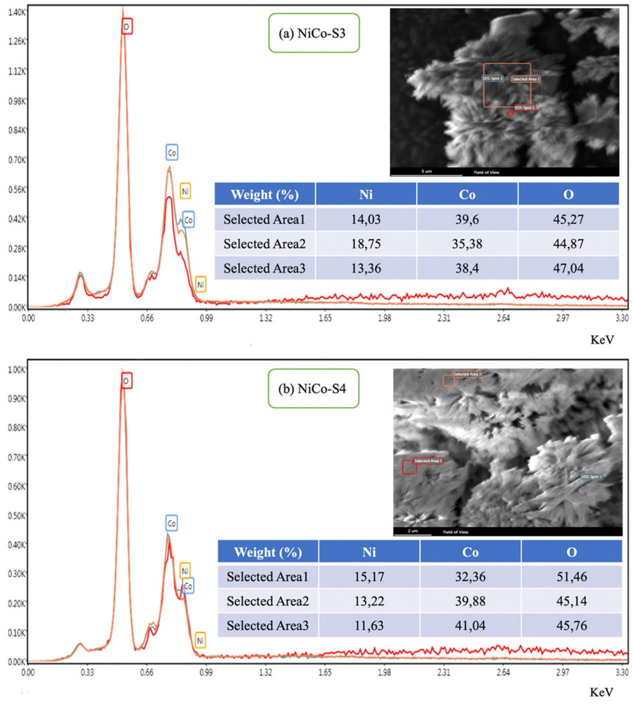

Weight (%)	Ni	Co	O
Selected Area1	14,03	39,6	45,27
Selected Area2	18,75	35,38	44,87
Selected Area3	13,36	38,4	47,04

Weight (%)	Ni	Co	O
Selected Area1	15,17	32,36	51,46
Selected Area2	13,22	39,88	45,14
Selected Area3	11,63	41,04	45,76

Fig. 4 EDS analysis of synthesised $NiCo_2O_4$: (a) NiCo-S3 and (b) NiCo-S4.

The NiCo-S3 and NiCo-S4 are further examined by using TEM, which can show the dispersion of particles, grain size, and morphology in nanometer dimensions. In Fig. 5, Fig. 5a is the TEM image of NiCo-S3, and Fig. 5b is the TEM image of NiCo-S4 on the scale of 50 nm. For both samples, after measuring their dimension distribution, their particle size is between 20 nm and 45 nm. The lattice spacing for NiCo-S3 and NiCo-S4 is 0.249 and 0.246 nm, respectively, which is related to the (311) plane of $NiCo_2O_4$. Also, for NiCo-S4 the lattice spacing of 0.203 nm which is related to the (400) plane was observed. These results confirm further what was obtained by SEM and EDS analysis and endorse the purity of the synthesized samples in nanometer dimensions.

3.1.3. Electrochemical performance of $NiCo_2O_4$ for the OER. In Fig. 6, the OER properties of freshly prepared

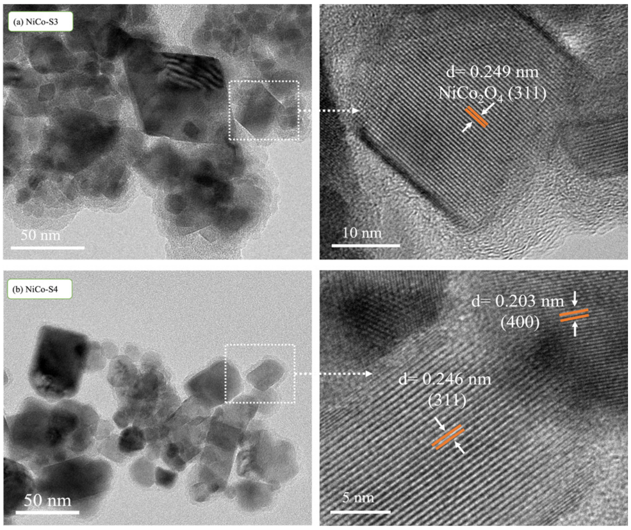

Fig. 5 TEM images of $NiCo_2O_4$: (a) NiCo-S3 and (b) NiCo-S4.

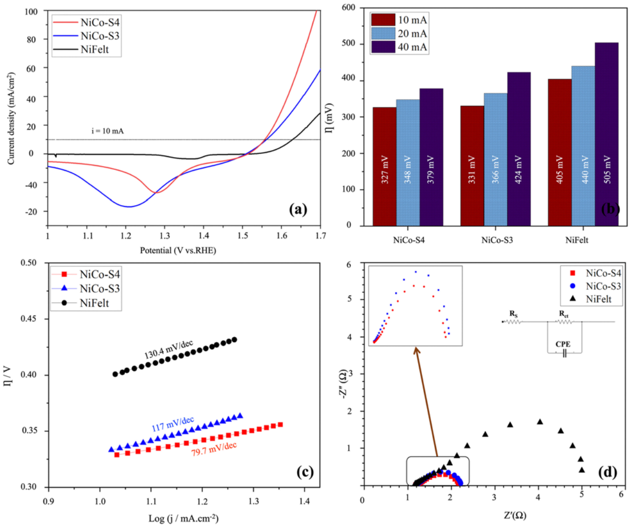

Fig. 6 OER property of NiCo-S3 and NiCo-S4 samples: (a) IR-corrected LSV plot, (b) overpotentials, (c) Tafel slopes, and (d) Nyquist plot.

NiCo-S3 on Ni felt, NiCo-S4 on Ni felt, and cleaned bare Ni felt are presented. These electrodes were used as anodes to evaluate their electrocatalytic performance for the OER in 1 M KOH solution as an electrolyte, while Hg/HgO was used as the reference electrode and a platinum foil as the counter electrode in a standard three-electrode setup. To evaluate the synthesized electrocatalyst performances on the Ni felt, backward linear sweep voltammetry (LSV) was conducted with a 5 mV s^{-1} scan rate, and the results of 80% *iR* corrected LSV are given in Fig. 6a. As can be seen, NiCo-S4 showed high electrochemical activity in comparison to NiCo-S3 and bare NiFelt. Considering the overpotential of the synthesized electrode at 10 mA cm^{-2}, NiCo-S4 has the lowest overpotential of 327 mV, which is followed by NiCo-S3 at 331 mV and NiFelt at 405 mV. By going deep into the overpotential differences between the synthesized electrodes, a comparison at different current densities is provided in Fig. 6b. At a current density of 20 mA cm^{-2}, the overpotential for NiCo-S4, NiCo-S3, and NiFelt is 348, 466, and 440 mV, respectively. By increasing the current density to 40 mA Cm^{-2}, the overpotential for NiCo-S3 and NiFelt increases significantly, while for NiCo-S4, it is just at about 379 mV. As expected, based on the results obtained by SEM and TEM, NiCo-S4 revealed lower overpotential in comparison to NiCo-S3 and NiFelt, which means that the electrochemical activity of NiCo-S4 is much higher. This is due to the existence of nanorods with homogeneous structures in a flower-shaped form, which can increase the specific surface area for electrochemical reactions. NiCo-S3 and NiCo-S4 have good performances in terms of overpotential if compared with other similar catalysts. The overpotential obtained by Kumar *et al.* on two $NiCo_2O_4$ samples (synthesized with a modified methodology using grape juice) was 290 mV and 260 mV, while a value of 300 mV was obtained for the pure $NiCo_2O_4$, synthesized for comparison with the two samples obtained by using grape juice, at a current density of 10 mA cm^{-2} in 1 M KOH.[43] Liu *et al.* obtained an overpotential of 490 mV at a current density of 10 mA cm^{-2} in 0.5 M H_2SO_4 electrolyte for $NiCo_2O4$ synthesized by co-electrodeposition on a graphite fiber support.[44] Qiao *et al.* obtained an overpotential of 370 mV at 10 mA cm^{-2} in 0.1 M KOH aqueous solution for $NiCo_2O_4$/CoNx-NMC (NMC = nitrogen doped mesoporous carbon), while a value of 290 mV of overpotential at 10 mA cm^{-2} was found in 1 M KOH by Gao *et al.* for the $NiCo_2O_4$ catalyst obtained by the solvothermal method on Ni foam.[45,46] A $NiCo_2O_4$ on graphite fiber has been obtained by electrodeposition by Liu *et al.*, reaching a value of 308 mV overpotential at 10 mA cm^{-2} in 1 M KOH.[47]

Moreover, by obtaining the Tafel slope based on backward LSV, the catalytic activity can be revealed by showing which electrode needs the lowest energy to be activated. In Fig. 6c, the Tafel slope for NiCo-S3, NiCo-S4, and NiFelt is depicted, which is 117, 79.7, and 130.4 mV dec^{-1}, respectively. The Tafel slope for NiCo-S4 at 79.7 mV dec^{-1} shows that this electrode has very good kinetics and needs lower energy to be activated in comparison to NiCo-S3 and NiFelt. NiCo-S4 shows a good performance in terms of Tafel slope, too, if compared with similar studies. Kumar *et al.* computed a Tafel slope of 99 and 95 mV dec^{-1} for the two modified samples, while it was 104 mV dec^{-1} for the standard $NiCo_2O_4$.[43] The Tafel slope obtained by Liu *et al.* in 1.0 M KOH on $NiCo_2O_4$ synthesized by co-electrodeposition on a graphite fiber support was 88 mV dec^{-1}.[47] Also, for $NiCo_2O_4$/CoNx-NMC (Nitrogen doped mesoporous carbon), $NiCo_2O_4$ on NiFoam prepared by the solvothermal method, and metallic NiCo nitride nanoparticle/$NiCo_2O_4$ nanoflake/graphite fibers synthesized *via* co-electrodeposition, the calculated Tafel slope was 99, 53, and 61 mV dec^{-1}, respectively.[45,46,48]

Furthermore, at the open circuit voltage, electrochemical impedance spectroscopy (EIS) was carried out to investigate the system's intrinsic transport characteristics. To assess the findings, an equivalent circuit was obtained by data analysis. Fig. 6d illustrates that the resistance measured at high frequencies is related to the uncompensated solution resistance (R_Ω), which is constant for all examined electrodes, at around 1.17 Ω. In particular, the semicircle diameter of the NiCo-S4 and NiCo-S3 electrodes, which is related to charge transfer resistance (R_{ct}), decreased considerably when compared to bare NiFelt, especially in the mid and low-frequency ranges. The R_{ct} for NiCo-S4, NiCo-S3, and NiFelt is 1.03, 1.16 and 3.516 Ω, respectively. This finding implies that the charge transfer kinetics of the NiCo-S4 and NiCo-S3 electrodes have been significantly improved and supports the results gathered through backward LSV and SEM analysis, which indicate that NiCo-S4 is an electrocatalyst with a lowered potential energy barrier for driving current through the catalyst, hence increasing OER efficiency. NiCo-S3 and NiCo-S4 also confirmed good behavior in this test. The EIS test done by Park *et al.* on $NiCo_2O_4$ obtained by direct growth *via* the hydrothermal method on graphite fiber gave an R_s of 2.768 Ω and an R_{ct} of 1.814 Ω.[49] Kaur *et al.* reported a $NiCo_2O_4$ obtained by co-precipitation, in which the R_s and R_{ct} were 0.684 and 4.64 Ω, respectively.[50]

In order to have an estimation of the electrochemical active surface area (ECSA), double layer capacitance (C_{dl}) is calculated based on cyclic voltammetry (CV) in the region where there is

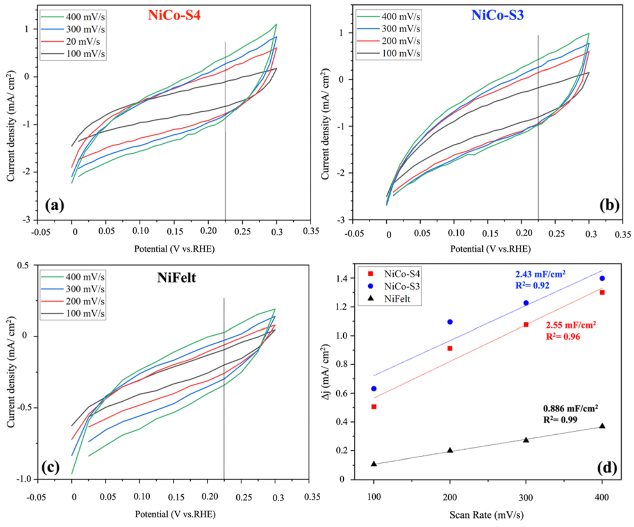

Fig. 7 CV curves of electrodes: (a) NiCo-S4, (b) NiCo-S3, and (c) NiFelt; (d) double-layer capacitance.

no Faraday potential, and the results are given in Fig. 7. For all the electrodes, including NiFelt, the potential range is between 0 and 0.3 V *vs.* RHE, and different scan rates starting from 100 mV s^{-1} to 400 mV s^{-1} were used to extract C_{dl} by depicting the linear relationship between current density and scan rate. From Fig. 7d, the C_{dl} for NiCo-S3, NiCo-S4, and NiFelt is 2.43, 2.55 and 0.886 mF cm^{-2}, respectively. These values were obtained by calculating the difference between cathodic and anodic peaks for each scan rate, which are plotted with a first-order model at 0.22 V *vs.* RHE, and the slope of each electrode corresponds to the C_{dl}. As the C_{dl} has a direct relationship with ECSA, an electrode that has higher C_{dl} will have higher ECSA, too. In this study, NiCo-S4 showed higher C_{dl}, which means that the electrochemical active surface area is higher when using this electrocatalyst in comparison to bare NiFelt and NiCo-S3. To have a comparison, Shuai *et al.* computed a C_{dl} of 2.6 mF cm^{-2} by performing a CV test in 1 M KOH electrolyte for $NiCo_2O_4$/RGO obtained by the precipitation method, which is near the value calculated for NiCo-S4 without using RGO.[51]

As an indicator of the intrinsic catalytic activity, turnover frequency (TOF) can be calculated to show the rate of oxygen produced per active site of the material based on the formula TOF = $j*A/(4*F*m)$, in which j is the current density at a specific potential (A cm^{-2}), A is the surface area of the electrode (1 cm^{-2}), F is the Faraday constant (96 485 C mol^{-1}), and m is the amount of active material (mol cm^{-2}).[52,53] TOF_{OER} for NiCo-S3 and NiCo-S4 is given in Table 2. As can be seen, the TOF for NiCo-S3 and NiCo-S4 is 1.69 and 2.51 (10^{-3} S^{-1}), respectively, with almost 48% higher TOF for NiCo-S4, in line with the results obtained by LSV, Tafel slope and ECSA.

Table 2 TOF value for NiCo-S3 and NiCo-S4

Name	Catalyst	Potential V. *vs.* RHE	Current density (mA cm^{-2})	TOF value (10^{-3} S^{-1})
NiCo-S3	$NiCo_2O_4$	1.6	21.71	1.69
NiCo-S4	$NiCo_2O_4$	1.6	32.25	2.51

Electrocatalytic stability is another critical element in determining the usability and performance of the synthesized catalysts; the results are provided for the selected best OER electrodes in Fig. 8. The stability test was performed at 10 mA cm^{-2} over 24 h for NiCo-S4, and the result is shown in Fig. 8e. The potential started at around 1.56 V *vs.* RHE, and at the end, it slightly decreased to about 1.553 V, which means that the electrocatalyst for the OER is stable. By comparing stability results with other works, Gao *et al.* synthesized a hierarchical $NiCo_2O_4$ hollow microcuboid by the hydrothermal method, the durability test was done under galvanostatic conditions at a current density of 10 mA cm^{-2} for 32 h, and the overpotential registered an increment of 10 mV, which is in accordance with NiCo-S4.[45] Liu *et al.* measured durability in a two electrode set-up by applying a current of 10 mA for 40 hours in 1.0 M KOH electrolyte for NiCo-nitrides/$NiCo_2O_4$/GF, and the test displayed a little degradation and an increase of potential while oxygen bubbles arose.[48] For two $NiCo_2O_4$ samples (modified with grape juice) reported by Kumar *et al.* the stability test over 40 h by chronoamperometry at 20 mA cm^{-1} in 1.0 M KOH for the best sample displayed negligible losses.[43]

Moreover, backward LSV was performed at the end of the 24 h and compared with the initial one. The results are

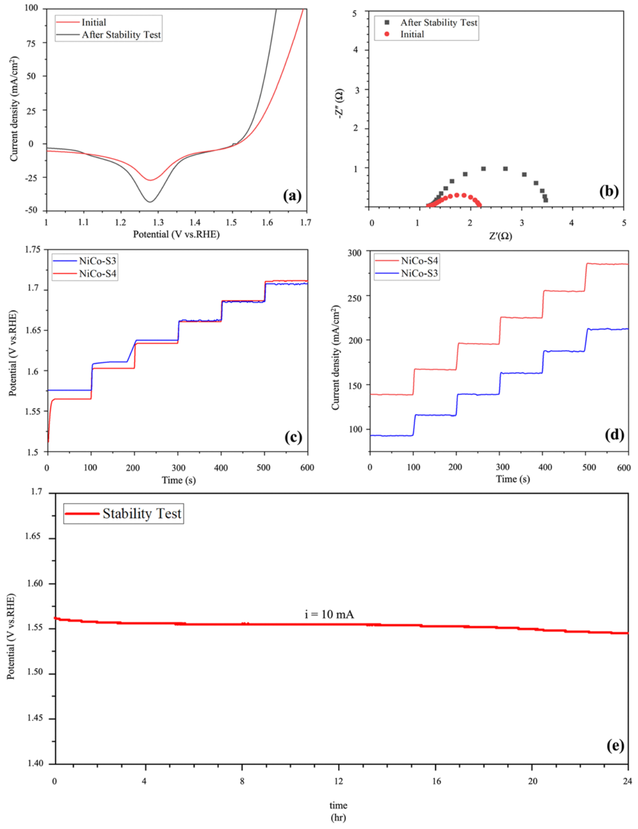

Fig. 8 Stability of electrodes: (a) CV curves of NiCo-S3 and NiCo-S4 after 500 cycles. (b) EIS of NiCo-S3 and NiCo-S4 after the stability test, (c) multipotential curve, (d) multicurrent curve, and (e) chronopotentiometric curve of NiCo-S4.

given in Fig. 8a. The backward LSV after the stability test showed higher activity than the initial one. This behavior could be related to the production of gas bubbles at the beginning of the process, which cannot diffuse from the pores of NiFelt to the solution media.

Furthermore, as the $NiCo_2O_4$ has super capacitance behavior, some energy is gathered to charge the electrode initially. Accordingly, more investigations were planned to verify the dimension of the bubbles attached to the electrodes as suggested by Huang *et al.*, and also the gas bubble removal method with pressure swing for foam electrodes, which is suggested and evaluated by Bleeker *et al.* by using fast pressure swing of N_2 gas under 1 second of time[54,55] Comparing the decay behavior with other relevant work, Kumar *et al.* performed the LSV after the stability test, which showed that the current density at 1.6 V is almost stable at about 120 mA cm^{-2} for $NiCo_2O_4$ modified with grape juice.[43]

The Nyquist plot for NiCo-S4 before and after the 24-hour stability test was recorded, and the results are depicted in Fig. 8b. Charge transfer resistance after the stability test increased to 2.15 Ω while for fresh NiCo-S4 it was 1.03 Ω. Comparing the results of EIS and LSV after the stability test shows that as NiCo-S4 is deposited in all volumes of the NiFelt, it is active and produces oxygen at a rapid pace inside the pores, which requires some time to desorb these bubbles to the electrolyte and achieve desired potential. On the other hand, higher R_{ct} after stability shows some detachments of this catalyst but not in a way to reduce the efficiency of electrochemical activity.

Besides the long-term durability of NiCo-S4, multi-potential as well as multi-current measurements were carried out for both NiCo-S4 and NiCo-*S*-3, and the results are presented in Fig. 8c and d. For chronopotentiometry (Fig. 8c), each step was performed for 100 s and started from 10 mA to 60 mA of current density. As can be seen, NiCo-S4 is more stable and reaches a lower potential, which means that it has lower resistance and higher electrochemical activity. On the other side, chronoamperometry was applied starting from 350 mV to 600 mV, and each step was carried out for 100 s, too. In this analysis, again, NiCo-S4 showed superior characteristics and achieved higher current when compared to NiCo-S3, and hence it was selected as the salient electrode for the OER process.

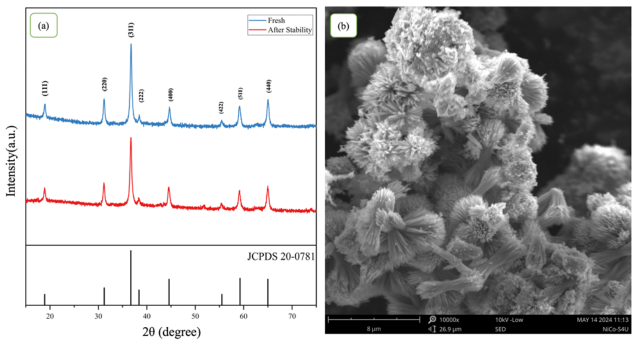

Fig. 9 Physicochemical analysis of NiCo-S4 after the stability test: (a) XRD of NiCo-S4 after the stability test and (b) SEM of NiCo-S4 after the stability test.

To have a better idea about the NiCo-S4 after the stability test, physicochemical analysis has been performed and the results are given in Fig. 9. The XRD analysis (Fig. 9a) showed no difference between the used and fresh NiCo-S4 electrocatalysts and aligned with the JCPDS No. 20-0781. Moreover, SEM analysis (Fig. 9b) showed that the mum-flower structure remained stable with small quantities of flower rods detached from this structure after the stability test but the material is $NiCO_2O_4$ and can be electrochemically active based on the results of the stability test.

4. Conclusions

In this work, eight samples of $NiCo_2O_4$ catalysts were synthesized by the hydrothermal method adopting different amounts of nucleating agent, and hydrothermal, and calcination temperatures. The study drove the selection of the two best samples first, from a morphological point of view: NiCo-S3 and NiCo-S4. The two samples showed a single-phase morphology with an urchin-like shape. TEM analyses displayed the outstanding result of obtained particle dimensions (20–45 nm). From the electrochemical tests, NiCo-S4 showed the most promising results: an overpotential of 327 mV at 10 mA cm^{-2}, a Tafel slope of 79,7 mV dec^{-1}, a low charge transfer resistance (R_{ct}) of 1.03 Ω and a C_{dl} of 2,43 mF cm^{-2}. The results displayed are meaningful and show the appropriate OER activity of this catalyst. Moreover, the stability test showed a retention of 99% of performances over 24 h. The LSV test after the stability test highlighted how performances slightly improved while the charge transfer resistance computed from EIS after the stability test doubled. From these results, it can be said that the electrode made with foam electrodes and felts needs a period to reach mass transport stability for removing bubbles. The study of the effects of the three key operating variables chosen as discriminating factors drove the selection of the best ones to synthesize the $NiCo_2O_4$ with the desired characteristics.

Author contributions

Ataollah Nyati: conceptualization, investigation, formal analysis, visualization, writing – original draft, writing – review & editing. Arianna Moranda: validation, formal analysis, writing – review & editing. Juan Felipe Basbus: analysis, investigation. Ombretta Paladino: writing – reviewing and editing, supervision, project administration, funding acquisition.

Conflicts of interest

There are no conflicts to declare.

Acknowledgements

The authors wish to thank Prof. Antonio Comite (Head of the Elemental lab at DCCI, Department of Chemistry of University of Genoa) and Mrs Laura Negretti who carried out TEM analyses at DCCI. The present work was funded by EU Next Generation - PNRR, M2C213.5, project NEMESI_ID: RSH2B_000002, and by the PhD grant FSE + 2021-2027, ESO 4.6 at the University of Genova, Italy.

Notes and references

1 T. Xu, Y. Wang, Y. Xue, J. Li and Y. Wang, *Chem. Eng. J.*, 2023, **470**, 144247.

2 D. Yu, X. Wan and B. Gu, *Chemosphere*, 2023, **323**, 138182.

3 H. A. Miller, K. Bouzek, J. Hnat, S. Loos, C. I. Bernäcker, T. Weißgärber, L. Röntzsch and J. Meier-Haack, *Sustainable Energy Fuels*, 2020, **4**, 2114–2133.

4 D. Henkensmeier, M. Najibah, C. Harms, J. Žitka, J. Hnát and K. Bouzek, *J. Electrochem. Energy Convers. Storage*, 2021, DOI: **10.1115/1.4047963**.

5 D. Gielen, F. Boshell, D. Saygin, M. D. Bazilian, N. Wagner and R. Gorini, *Energy Strategy Rev.*, 2019, **24**, 38–50.

6 F. Van Der Linden, E. Pahon, S. Morando and D. Bouquain, *J. Power Sources*, 2023, **575**, 233168.

7 S. Huang, Z. Yuan, M. Salla, X. Wang, H. Zhang, S. Huang, D. G. Lek, X. Li and Q. Wang, *Energy Environ. Sci.*, 2023, **16**, 438–445.

8 G. Yang, Y. Zhu, Z. Hao, Y. Lu, Q. Zhao, K. Zhang and J. Chen, *Adv. Mater.*, 2023, **35**(33), DOI: **10.1002/adma.202301898**.

9 S. Bonizzoni, D. Stucchi, T. Caielli, E. Sediva, M. Mauri and P. Mustarelli, *ChemElectroChem*, 2023, **10**(6), DOI: **10.1002/celc.202201077**.

10 P. Hota, A. Das and D. K. Maiti, *Int. J. Hydrogen Energy*, 2023, **48**, 523–541.

11 L. Lu, Y. Zheng, R. Yang, A. Kakimov and X. Li, *Mater. Today Chem.*, 2021, **21**, 100488.

12 B. Guo, Y. Ding, H. Huo, X. Wen, X. Ren, P. Xu and S. Li, *Nanomicro. Lett.*, 2023, **15**, 57.

13 L. Yang, J. Shui, L. Du, Y. Shao, J. Liu, L. Dai and Z. Hu, *Adv. Mater.*, 2019, **31**, 1804799.

14 A. Moysiadou and X. Hu, *J. Mater. Chem. A*, 2019, **7**, 25865–25877.

15 F. Song, L. Bai, A. Moysiadou, S. Lee, C. Hu, L. Liardet and X. Hu, *J. Am. Chem. Soc.*, 2018, **140**, 7748–7759.

16 H. Osgood, S. V. Devaguptapu, H. Xu, J. Cho and G. Wu, *Nano Today*, 2016, **11**, 601–625.

17 J. X. Flores-Lasluisa, F. Huerta, D. Cazorla-Amorós and E. Morallón, *Environ. Res.*, 2022, **214**, 113731.

18 X.-M. Liu, X. Cui, K. Dastafkan, H.-F. Wang, C. Tang, C. Zhao, A. Chen, C. He, M. Han and Q. Zhang, *J. Energy Chem.*, 2021, **53**, 290–302.

19 Q. Zhao, Z. Yan, C. Chen and J. Chen, *Chem. Rev.*, 2017, **117**, 10121–10211.

20 S. Liu, L. Hu, X. Xu, A. A. Al-Ghamdi and X. Fang, *Small*, 2015, **11**, 4267–4283.

21 L. Hu, L. Wu, M. Liao, X. Hu and X. Fang, *Adv. Funct. Mater.*, 2012, **22**, 998–1004.

22 C. Peng, H. Liu, J. Chen, Y. Zhang, L. Zhu, Q. Wu, W. Zou, J. Wang, Z. Fu and Y. Lu, *Appl. Surf. Sci.*, 2021, **544**, 148897.

23 W. Sudarsono, S. Y. Tan, W. Y. Wong, F. S. Omar, K. Ramya, S. Mehmood, A. Numan, R. Walvekar and M. Khalid, *J. Ind. Eng. Chem.*, 2023, **122**, 1–26.

24 Z. Wu, X. Pu, Y. Zhu, M. Jing, Q. Chen, X. Jia and X. Ji, *J. Alloys Compd.*, 2015, **632**, 208–217.

25 D. Yadav, P. Singh and R. Prasad, *Int. J. Hydrogen Energy*, 2019, **44**, 29057–29065.

26 M. Kaur, P. Chand and H. Anand, *J. Energy Storage*, 2022, **52**, 104941.

27 M. Kaur, P. Chand and H. Anand, *Chem. Phys. Lett.*, 2022, **786**, 139181.

28 S. Yan, S. Luo, M. Sun, Q. Wang, Y. Zhang and X. Liu, *Int. J. Energy Res.*, 2021, **45**, 20186–20198.

29 E. Abbasi, M. Haghighi, M. Shabani, A. Niyati and S. Mahboob, *Mater. Today Sustainability*, 2023, **24**, 100580.

30 B. Sriram, S. Kogularasu, S.-F. Wang and J.-K. Sheu, *ACS Appl. Nano Mater.*, 2023, **6**, 17593–17602.

31 J. I. Orege, J. Wei, Q. Ge and J. Sun, *Nano Today*, 2023, **51**, 101914.

32 Y. Zhang, W. Zhang, J. Zhou, X. Li, W. Zhou, Y. Xie, J. Mao and K. Dai, *J. Electrochem. Soc.*, 2023, **170**, 090532.

33 A. Niyati, M. Haghighi and M. Shabani, *Mater. Today Sustainability*, 2023, **24**, 100478.

34 H. Fu, L. Chen, Y. Shi, W. Kong, X. Zhang, J. Hou, H. Li, G. Wang, F. Yu and X. Guo, *Electrochim. Acta*, 2019, **320**, 134581.

35 H. Fu, Y. Liu, L. Chen, Y. Shi, W. Kong, J. Hou, F. Yu, T. Wei, H. Wang and X. Guo, *Electrochim. Acta*, 2019, **296**, 719–729.

36 M. Chatterjee, S. Saha, S. Das and S. K. Pradhan, *J. Alloys Compd.*, 2020, **821**, 153503.

37 S. Yadav, A. Sharma Ghrera and A. Devi, *Mater. Today Proc.*, 2023, **74**, 281–288.

38 R. Packiaraj, P. Devendran, K. S. Venkatesh, K. Mahendraprabhu and N. Nallamuthu, *J. Energy Storage*, 2021, **34**, 102029.

39 X. Zhang, F. Yang, H. Chen, K. Wang, J. Chen, Y. Wang and S. Song, *Small*, 2020, **16**(44), DOI: **10.1002/smll.202004188**.

40 G. Yang and S.-J. Park, *Electrochim. Acta*, 2018, **285** 405–414.

41 Z.-Q. Liu, Q.-Z. Xu, J.-Y. Wang, N. Li, S.-H. Guo, Y.-Z. Su, H.-J. Wang, J.-H. Zhang and S. Chen, *Int. J. Hydrogen Energy*, 2013, **38**, 6657–6662.

42 W. Zheng, *ACS Energy Lett.*, 2023, **8**, 1952–1958.

43 S. Kumar, A. Tahira, M. Emo, B. Vigolo, A. Infantes-Molin, A. M. Alotaibi, S. F. Shaikh, A. Nafady and Z. H. Ibupoto, *J. Energy Storage*, 2023, **68**, 107708.

44 Z. Liu, H. Tan, D. Liu, X. Liu, J. Xin, J. Xie, M. Zhao, L. Song, L. Dai and H. Liu, *Adv. Sci.*, 2019, **6**(5), DOI: **10.1002/advs.201801829**.

45 X. Gao, H. Zhang, Q. Li, X. Yu, Z. Hong, X. Zhang, C. Liang and Z. Lin, *Angew. Chem., Int. Ed.*, 2016, **55**, 6290–6294.

46 M.-F. Qiao, Y. Wang, L. Li, G.-Z. Hu, G.-A. Zou, X. Mamat, Y.-M. Dong and X. Hu, *Rare Met.*, 2020, **39**, 824–833.

47 Z. Liu, H. Tan, D. Liu, X. Liu, J. Xin, J. Xie, M. Zhao, L. Song, L. Dai and H. Liu, *Adv. Sci.*, 2019, **6**(5), DOI: **10.1002/advs.201801829**.

48 Z. Liu, H. Tan, D. Liu, X. Liu, J. Xin, J. Xie, M. Zhao, L. Song, L. Dai and H. Liu, *Adv. Sci.*, DOI: **10.1002/advs.201801829**.

49 H. Park, B. H. Park, J. Choi, S. Kim, T. Kim, Y.-S. Youn, N. Son, J. H. Kim and M. Kang, *Nanomaterials*, 2020, **10**, 1727.

50 M. Kaur, P. Chand and H. Anand, *Chem. Phys. Lett.*, 2022, **786**, 139181.

51 C. Shuai, Z. Mo, X. Niu, X. Yang, G. Liu, J. Wang, N. Liu and R. Guo, *J. Mater. Sci.*, 2020, **55**, 1627–1636.

52 Y. Cheng, P. Fu, X. Yang, Y. Zhang, S. Jin, H. Liu, Y. Shen, X. Guo and L. Chen, *J. Mater. Chem. A*, 2023, **11**, 24764–24776.

53 Y. Zheng, L. Wang, J. Pang, K. Sun, J. Hou, G. Wang, W. Guo and L. Chen, *J. Colloid Interface Sci.*, 2023, **637**, 85–93.

54 C. Huang, Z. Wang, Z. Yao, Y. Ma, F. Guo and L. Chai, *Electrochim. Acta*, 2024, **477**, 143792.

55 J. Bleeker, C. van Kasteren, J. R. van Ommen and D. A. Vermaas, *Int. J. Hydrogen Energy*, 2024, **57**, 1398–1407.